B. 研究方法

1. 試料調整

爆発法で作成されたナノダイヤモンド(ND)(ナノ炭素研究所)をシリコン基盤上に塗布した後、100keVのMn＋を$5x10^{15}/cm^2$、$1x10^{16}/cm^2$、$3x10^{16}/cm^2$打ち込んだ(Mn-ND)。その後、アニール処理、空気参加処理を順次施した。合成された磁性NDの物性は、Spring-8での軟X線分光法、硬X線分光法に、より、それぞれ調べた。

2. MRI測定

イオン注入したND(Mn-ND)は、超音波洗浄機で、破砕した後、使用した。

マウスでの実験は、11.7T MRI (Bruker製)を用いて行った。T_1強調画像は、FLASH法を用いた。Mn-NDの生体内での造影能を評価するため、2種類の実験を行った。ひとつは、鼠径リンパ節に直接投与する実験、もう一つは、マウス背足部から投与し、投与後、1時間にMRI撮像を行い、膝下リンパ節への移行を調べた。

3. 軟X線分光

イオン注入後のND内部でのC、およびMnイオンの電子状態を調べるために、L殻励起吸収スペクトルを取得し、注入後の処理条件の検討、および処理後の2価のMnイオンの割合を探ることを目的とした。入射光に水平な面内に光電子分析器と軟X線発光分光器を配置する。光電子分析器は、Au4fを用いた入射光エネルギー補正、及び高次光補正用に用いる。試料面への入射角は斜入射70°に固定する。軟X線発光分光器のエネルギー軸及び分解能調整にはSiO2鏡面の乱反射スペクトルを用いる。試料には、$1x10^{16}/cm^2$のMnイオンを注入した4nmのナノダイヤモンドND(Mn-ND as impla.)とアニールしたもの(Mn-ND with anneal)、さらにアニール後にさらに空気酸化したものとアニールせずに空気酸化したもの(Mn-ND with anneal +air oxidation)を用いた。サンプルは、$10mm^2x0.5mm$程度の大きさのペレットとした。これらの試料のMn L-edge 軟X線発光および蛍光スペクトルを、BL27SUを用いて、イオン注入後の処理過程の注入Mnイオンの電子状態への影響の効果を調べた。測定は室温で行った。

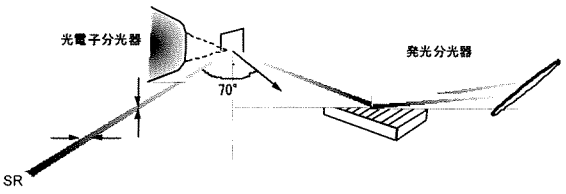

図1:発光分光時の放射光と試料配置

次に、アニール温度依存的な磁性センターの形成状態を調べるため、300、400、500、600、700、800、1000℃で2時間アニール処理したMn-NDのMn L-edge 軟X線吸収分光測定を行った。

これらの測定は、いままでの全蛍光収量法ではなく、元素選択的な部分蛍光収量法で行った。

4. 硬X線吸収分光

イオン注入後のND内部でのMnイオンの炭素原子との結合状態を調べるために、MnのK殻XAFSスペクトルを取得し、その安定性の構造基盤を探ることを目的とした。

試料には、$1x10^{16}/cm^2$のMnイオンを注入した直後の4nmのナノダイヤモンドND(Mn-ND-ai)とアニールしたもの(Mn-ND-a)、さらにアニール後にさらに空気酸化したものとアニールせずに空気酸化したもの(Mn-ND-ao)を用いた。サンプルは、$10mm^2x0.5mm$程度の大きさのペレットとした。これらの試料のMn K-edge X線吸収スペクトルを、BL14を用いて測定した。測定は室温で行った。

C. 研究結果

1. Mn-NDのイオン注入後のMnイオンの電子状態とその安定構造についてのより詳細な解析

いままでにNDへのMnイオン注入後のサンプルに対したESR及びMRIを観測したところ、2価イオンの存在を示すシグナルが現れることがわかっている。このことは、1価で注入したイオンが、ND内部のsp3的(ダイアモンド的)な環境において、何らかの理由で2価で安定に存在することを意味している。実際、MRIに効果を持つのは、いずれも2価の常磁性イオンになった場合のみであり、その2価イオンとしての安定性の原因を解明することは、効率的なイオン注入法の開発に役に立つと考えられる。

このため、イオン注入後のMnイオンの電子状態について、放射光分光で調べてきた。とくに、Mn L端軟X線吸収分光が有用であることが分かったが、Mn以外のCなどND中に含まれるすべての元素からの信号が含まれる全蛍光吸収法での分光法だったため、定量的な詳細な理解が難しかった。

そこで本年度は、JASRIの為則博士により導入されたMn元素だけの信号を抽出する部分蛍光吸収法により、L端Mn軟X線吸収分光を行った。

測定の結果、以下のことが分かった。1. イオン注入直後のMnイオンは、2価と3価が共存した(黒) 2. 真空中での700℃、2時間のアニールにより、MnOのスペクトル(青)とピークが一致した(赤)ことから、ほぼすべてのMnイオンが2価の状態になった 3. アニール後の425℃、5時間の空気酸化でも、Mnイオンは2価のままで、変化しなかった(緑)。4. さらに、641.5eV、および643eVの2つのエネルギーでのピークの伸長が顕著であった。643eVの信号は、metal to ligand charge transfer (MLCT)による効果と予想された。

これらの事実から、MRIに効果があると期待される常磁性イオンである2価の電子状態をとるようにするには、アニールが必要であり、この処理により注入イオンのほぼすべてが2価に変化していることが分かった。以上の結果から、イオン注入法による簡便なMRI造影剤合成法が確立されたといえる。

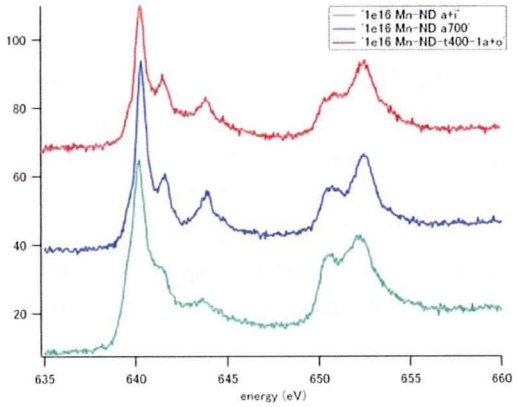

図2:SPring-8で取得したMn2p吸収スペクトル(XAS) 部分蛍光収量法により、測定時間の短縮が可能になり、今後の効率的な造影剤開発に有用な方法論が確立された。

ここにイオン注入後の処理方法について確立したが、こうした方法が、注入イオン量を増やした場合の安定な常磁性センター形成の定量化にも利用できるかどうか調べるため、注入イオン量(5e15、1e16、3e16/cm^2)を変化させた試料を、アニールと空気酸化を施した後、軟X線吸収分光を行った。

その結果、イオン注入量に依存して、信号増強が見られた。このことは、3e16/cm^{2}までは、MRIに効果のあるほとんどの注入イオンがMRIに効果のある2価の電子状態を取れることを意味し、今後は、どの程度までMnイオン注入量を増加させることができるかを、軟X線吸収分光での信号を指標に検討していく予定である。

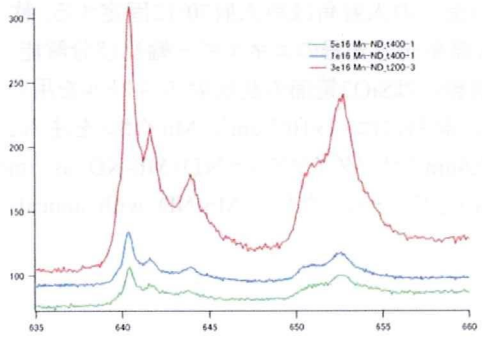

図3:異なるMnイオン注入量のNDの2p吸収スペクトル(XAS)

次に、注入Mnイオンがほとんど2価の状態になるアニール温度について軟X線吸収分光を用いて、さらに調べた。

その結果、以下のことが分かった。1．500℃以上のアニール温度で、注入したMnイオンがほとんど2価の状態になっていると考えられるスペクトルになった　3．642eVあたりのピークを指標に比較すると、700℃までは、アニール温度を上げると、信号強度が大きくなるが、800℃になると逆に信号強度が低下した。以上の結果は、Mnが2価状態になるには、600～700℃程度でアニールするとよいが、それ以上の温度でアニールする

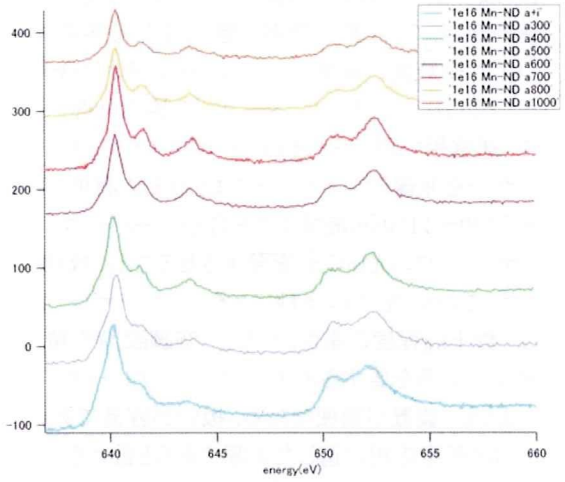

図4：異なるアニール温度でのXASスペクトラム

こうしたアニール温度の注入Mnイオンに与える効果をより、構造的に確認するため、硬X線吸収微細分光法で確認した。

その結果、以下のことが分かった。1．イオン注入直後の動径分布関数は、1つのピークしか見られなかった(水色)　2．真空中での300、400、500、600、700、800、1000℃、2時間のアニールにより、徐々に第一、および第二近接のピークが見られるようになった。とくに、300℃と400℃のアニール温度で、顕著な動径分布関数の変化が見られ、400℃で、第一、および第二近接のピークが見られるようになった。その後、第一近接のピークは、600～700℃まで増加するが、800℃以上になると低下した。

以上の結果から、アニール処理の注入Mnイオンに対する電子状態、および構造学的な評価から、イオン注入法後の効率的なMRI造影剤合成法に関する指針が得られたいえる。

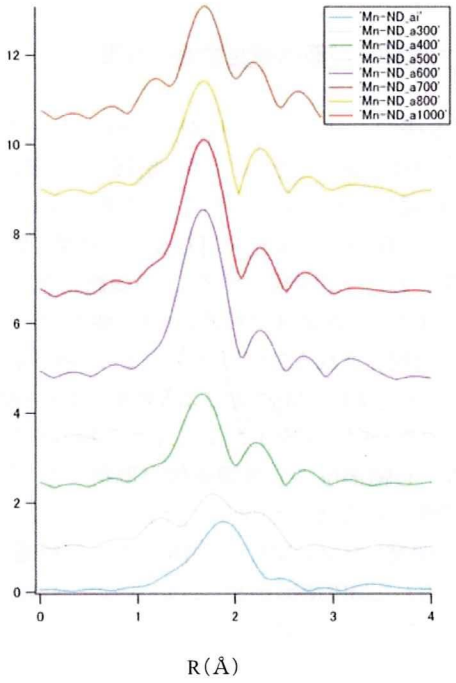

図5．イオン注入後の各処理による動径分布関数の変化

2．生体内長期安定型光・磁場応答性マルチモーダル用分子プローブの開発の継続と表面修飾による毒性の低減と生体応用

細胞内長期安定化プローブを開発し、生体内での標的細胞検出とその細胞集団のメタボノミクスをMRSで行うことを目指す。このため、現在完成した磁性・蛍光NDを長期安定性プローブにするための表面修飾法についてとくに検討した。まず、NDそのものへ金ナノ粒子を付加させ、その後PEGにより、生理環境下での分散性を維持できるか確認したところ、成功した。

その後、Mn-NDへも同様に表面上に付加することで、同様に生理環境下での分散性を維持できるか確認したところ成功し、血管造影剤として機能することが分かった。

臨床機でよく使用さている1.5T　MRI装置での血管造影できることが分かったことから、いままでのSPIOでは、信号低下のため難しい血管造影も同時にできる可能性を

示しており、Mn-NDの多様な展開が期待できる。

3. マウスリンパ節内細胞動態の可視化

本研究の目的である長期安定性プローブの有効性を調べるため、マウス鼠径リンパ節に光・磁場応答性ND分子プローブを取り込ませ、その経時的な変化を可視化した結果、数時間にわたって可視化することが確認できた。現在までに、背足部に投与しても、膝下リンパ節が可視化されることが分かっており、樹状細胞により込まれたMn-NDによる効果であると期待される。また、前述したようにivから投与した結果、心臓部位のT_1強調画像が取得でき、血管造影にも成功した(図6)。以上のことから、今回開発したMn-NDは，生体内でのT1短縮能を有したMRI造影剤としては、少なくとも有用であることが分かった。

図6. マウスリンパ節にNn-NDを注入後、1時間後にT_1強調画像で取得した図 鼠径リンパ節特有の瓢箪状の形状(右下の白い部分)が見られた。

3. 臨床機MRI装置内への組み込みを目指した蛍光・MRI同時計測デバイスの開発

昨年度までに11.7T高磁場MRI装置内で生体レベルのMRI画像と細胞レベルの蛍光画像を同時取得するため、RFコイル内にマウス・ラット等のモデル動物へファイバーを用いて近赤外領域の波長(690~1020nm;Spectra Physics社Maitai)のフェムト秒レーザー刺激光を伝送するファイバーシステムを構築した。今年度は、臨床機への展開を目指して、いままでのシステム以外に、新たに新規フェムト秒ファイバーレーザーによる光学システムを構築した。前年度までに、チタンサファイア結晶を用いたフェムト秒レーザーをMRIと融合するための光学系等を構築したが、システム構築を行った実験室から、実験用MRI装置、および臨床オープンMRIなど別棟にあるサイトに移動する際に、レーザー電源を落として、100kg以上ある装置を移動することは、開発を進めるうえで、非常に効率が悪く、また光学系のずれや装置の破壊がにつながるおそれがあることが分った。そこで、メーカーの協力を得て、通信用で用いられるErドープファイバーレーザーを非線形ファイバーにより当初の目的である700～1100nm帯域までを含むスーパーコンティニュウム光(SC光)を発生させることに成功した。このSC光フェムト秒ファイバーレーザーは、数十kg程度の重さしかなく、空調設備や精密な光学系を要するチタン・サファイアレーザーよりも、装置が簡便なため、扱いが容易であり、より医療応用に適した光源であると言える。今後は、2年目までに、現在製作中の内視鏡システムで画像が取得可能かを検討後、臨床用MRI装置での動作確認を行っていく予定である。

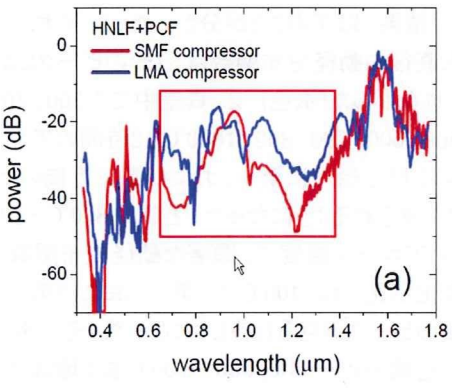

図7:MR対応ファイバーレーザーからの出力される広帯域波長の光

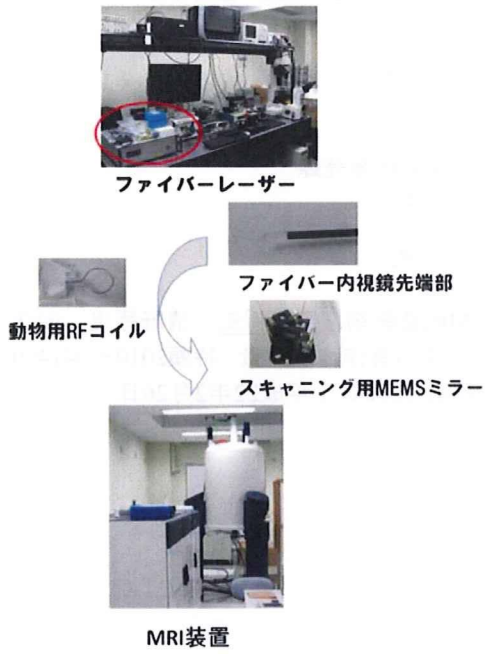

図8：共同で開発したMR対応ファイバーレーザーの構成と概観、
およびSC、いままでの複雑な光学系をほとんどをファイバ化し、移動や保守を簡素化することで、臨床応用につなげる。出力部もファイバー化されているため、内視鏡装置への接続や、MRI装置へ組み込みが容易である。さらに図7に示したSC光化により650~1400nmまでのフェムト秒パルスを一度に利用可能になり、生体深部のがん細胞の可視化も可能になると期待できる。

D. 考察

高齢者の医療費削減が急務な今日、多様な情報の取得による画像診断技術の進歩や診断精度向上とともに、予防医学の進展が求められている。本研究プロジェクトでは、高齢者でも負担の少ない患者さんにやさしい低侵襲な予防医学的診断手法の開発を目指し、一度に多様な情報を取得でき、さらに低侵襲かつ感度のよい蛍光画像とMRIを同時に取得するデバイスを開発してきた。さらに、細胞・分子ラベリング用プローブとして、生体適合性の高いと期待される炭素原子からなるナノダイヤモンド(ND)の表面修飾、および常磁性イオン注入による内部改変により、上記問題点を解決する光・磁場応答性分子プローブ(Magneto-Optical NAnodiamond; MONAD)を創製することを目指し、その合成に成功した。この造影剤は、常磁性イオンが、NDの内部に含まれるため、長期間トラッキングで問題となる金属イオンの毒性を回避しつつ、MR画像が取得できる。さらに蛍光色素の付加により細胞形態も可視化できる。これらの技術が開発できれば、細胞治療、とくにがん細胞をキラーT細胞によ り攻撃するための樹上細胞療法の効率化や、アルツハイマー病の進行を止めるためにミクログリアによるアミロイドプラークの除去や治療に重要であると短時間に多様な情報を取得でき、高齢者でも負担の少ない患者さんにやさしい予防医学的画像診断法の確立につながり、健康寿命を延ばす結果をもたらすと期待される。MRIと蛍光を同時に取得することは、予防医学的見地からも重要で、経時的な画像データによる観察から、疾患になりやすい部位の予測が可能になり、効率的な投薬が可能になる。また、病態解析時、とくに癌においては、癌細胞の転移状態と浸潤具合を一度に検査することが可能になると期待される。

とくに、今後、PET装置とのマルチモーダルイメージング装置開発を進めることで、分子・細胞イメージング技術の臨床展開が進んでいくことが期待される。

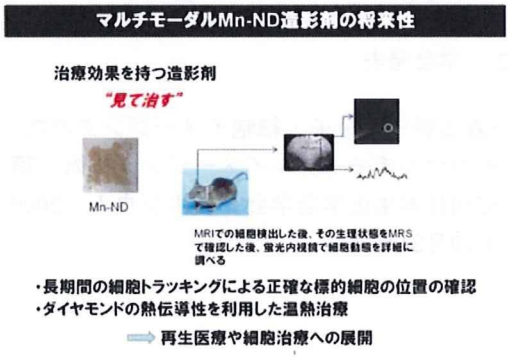

図10：マルチモーダルMn-NDの今後の展開

E. 結論

NDへのイオン注入法によるMRI造影剤合成法という新しい造影剤合成法を提案し、T_1短縮効果を持つND粒子の合成に成功した。

F. 健康危険情報

特記すべきことなし。

G. 研究発表

1. 論文発表

1) Preparation of Fluorescent Diamond Nanoparticles Stably Dispersed under a Physiological Environment through Multistep Organic Transformations. Takimoto T, Chano T, Shimizu S, Okabe H, Ito M, Morita M, Kimura T, Inubushi T and Komatsu N. Chemistry of Materials 22, 3462-3471 (2010)

2) Preparation for Highly Sensitive MRI Contrast Agents Using Core/Shell Type Nanoparticles Consisting of Multiple SPIO Cores with Thin Silica Coating. Tanaka K, Narita A, Kitamura N, Uchiyama W, Morita M, Inubushi T, Chujo Y. Langmuir. 26, 11759–11762 (2010)

3) Simple PEG conjugation of SPIO via an Au-S bond improves its tumor targeting potency as a novel MR tumor imaging agent. Kojima H, Mukai Y, Yoshikawa M, Kamei K, Yoshikawa T, Morita M, Inubushi T, Yamamoto TA, Yoshioka Y, Okada N, Seino S, Nakagawa S.
Bioconjug Chem. 21:1026-31 (2010).

2. 学会発表

・森田将史，分子・細胞イメージングのためのマルチモーダルイメージング技術、第82回日本生化学会学会シンポジウム、2009年10月21日

H. 知的財産権の出願・登録状況（予定を含む。）

1. 特許取得
なし

2. 実用新案登録
なし

3.その他

MRI造影剤、森田将史、清野智史、向洋平、中川晋作、中川貴. 特願2010－041460 (2010) 出願日：平成22年2月26日

研究成果の刊行に関する一覧表

書籍

著者氏名	論文タイトル名	書籍全体の編集者名	書　籍　名	出版社名	出版地	出版年	ページ
森田将史	マルチモーダル生体分子・細胞イメージングへの応用	磯部徹彦	ナノ蛍光体の開発と応用	シーエムシー出版	東京	2007	262-269

雑誌

発表者氏名	論文タイトル名	発表誌名	巻号	ページ	出版年
Takata K, Kitamura Y, Yanagisawa D, Morikawa S, Morita M, *et al.*	Microglial transplantation increases the Amyloid-ß clearance in Alzheimer model rats.	*FEBS Lett.*	581	475-478	2007
Yanagisawa D, Kitamura Y, Inden M, Takata K, Taniguchi T, Morikawa S, Morita M, *et al.*	DJ-1 protects against neurodegeneration caused by focal cerebral ischemia and reperfusion in rats.	Journal of Cerebral Blood Flow & Metabolism.	28	563-578	2008
Takimoto T, Chano T, Shimizu S, Okabe H, Ito M, Morita M, *et al.*	Preparation of Fluorescent Diamond Nanoparticles Stably Dispersed under a Physiological Environment through Multistep Organic Transformations.	Chemistry of Materials	22	3462-3471	2010
Kojima H, Mukai Y, Yoshikawa M, Kamei K, Yoshikawa T, Morita M, *et al.*	Simple PEG conjugation of SPIO via an Au-S bond improves its tumor targeting potency as a novel MR tumor imaging agent.	Bioconjug Chem.	26	11759-11762	2010
Tanaka K, Narita A, Kitamura N, Uchiyama W, Morita M, *et al.*	Preparation for Highly Sensitive MRI Contrast Agents Using Core/Shell Type Nanoparticles Consisting of Multiple SPIO Cores with Thin Silica Coating.	Langmuir	21	1026-1031	2010

FEBS Letters 581 (2007) 475–478

Microglial transplantation increases amyloid-β clearance in Alzheimer model rats

Kazuyuki Takata[a], Yoshihisa Kitamura[a,*,1], Daijiro Yanagisawa[a], Shigehiro Morikawa[b], Masahito Morita[b,e], Toshiro Inubushi[b], Daiju Tsuchiya[a], Saori Chishiro[a], Mana Saeki[a], Takashi Taniguchi[a], Shun Shimohama[c], Ikuo Tooyama[d,*,1]

[a] *Department of Neurobiology and 21st Century COE Program, Kyoto Pharmaceutical University, Misasagi, Yamashina-ku, Kyoto 607-8414, Japan*
[b] *Biomedical MR Science Center, Shiga University of Medical Science, Seta Tsukinowa-cho, Otsu 520-2192, Japan*
[c] *Department of Neurology, Sapporo Medical University, School of Medicine, S1W17, Chuo-ku, Sapporo 060-8556, Japan*
[d] *Molecular Neuroscience Research Center, Shiga University of Medical Science, Seta Tsukinowa-cho, Otsu 520-2192, Japan*
[e] *PRESTO, Japan Science and Technology Agency, 4-1-8 Honcho Kawaguchi, Saitama 332-0012, Japan*

Received 1 December 2006; revised 29 December 2006; accepted 8 January 2007

Available online 16 January 2007

Edited by Jesus Avila

Abstract Immunization with amyloid-β (Aβ) peptides, a therapeutic approach in Alzheimer's disease (AD), reduces brain Aβ, and microglial Aβ phagocytosis has been proposed as an Aβ-lowering mechanism. We transplanted rat microglia into the rat lateral ventricle just after intra-hippocampal Aβ injection, and then investigated the contribution of exogenous microglia to Aβ clearance. Migration of exogenous microglia from the lateral ventricle to Aβ plaque was detected by magnetic resonance imaging and histochemical analysis, and the clearance of Aβ was increased by transplantation. These results suggest the possible usefulness of exogenous microglia to the therapeutic approach in AD.

Keywords: Alzheimer's disease; Microglia; Amyloid-β peptide; Transplantation; Phagocytosis; Magnetic resonance imaging

1. Introduction

Accumulation of amyloid-β (Aβ) is a pathological hallmark of Alzheimer's disease (AD) and is thought to be a primary event in AD pathologies in the amyloid hypothesis [1]. On the other hand, accumulated Aβ in AD brains is surrounded by activated microglia [2]. Among recent studies that support the amyloid hypothesis, immunization with Aβ peptides using transgenic mouse models of AD indicated the effective reduction of brain Aβ and restoration of cognitive functions [3–6]. Microglial Aβ phagocytosis has been proposed as an Aβ-lowering mechanism of Aβ immunization, and Aβ phagocytosis of exogenously administered microglia was indicated in experimental ex vivo study using unfixed brain sections from both AD cases and transgenic mice [4]. These findings suggest the potential of exogenous microglia for the cell therapeutic approach in AD; however, experimental evidence is insufficient to consider whether the phagocytic function of exogenous microglia effectively contributes to Aβ clearance in in vivo brains.

2. Materials and methods

2.1. Alzheimer model rat and microglial transplantation

Animal experiments were carried out in accordance with the guidelines of the National Institutes of Health, and protocols were approved by the Committee for Animal Research at Kyoto Pharmaceutical University. For stereotaxic microinjection, male Wistar rats were immobilized in a Kopf stereotaxic frame. Coordinates were set according to a rat brain atlas [7]. Rats were microinjected with saline and 1 μg of synthetic human Aβ1-42 (Aβ42) peptide (AnaSpec) into the right and left hippocampus, respectively (i.e., 3.8 mm caudal from the bregma, 2.0 mm right and left lateral, 4.0 mm ventral, Fig. 1B). Lyophilized human Aβ42 was dissolved at a high concentration and aliquots were kept at −80 °C. Subsequently, Aβ42 was diluted with phosphate-buffered saline (PBS), and then immediately injected into the rat hippocampus. Microglial pure culture was prepared as described previously [8]. For magnetic resonance imaging (MRI), microglia (over 97% pure) were labeled with super-paramagnetic iron particles (Resovist; Nihon Schering K.K.) using the hemagglutinating virus of Japan envelop (HVJ-E; GenomONE, Ishihara Sangyo Kaisha Ltd.) vector as described previously [9]. Resovist-labeled microglia (Fig. 1A, inset) were re-suspended in PBS to a final concentration of approximately 1.0×10^6 cells in 5 μl, and then transplanted to the left lateral ventricle (i.e., 0.2 mm caudal from the bregma, 1.2 mm left lateral, 3.8 mm ventral, Fig. 1A) just after Aβ injection.

2.2. MRI

At one and eight days after Aβ42 and microglial injection, magnetic resonance (MR) images were acquired with a 7T Unity Inova MR scanner (Varian). Gradient echo images of the rat brain were acquired in sequential 8 slices of 1-mm thickness of the coronal plane with 300-ms repetition time, 15-ms echo time, 30° flip angle, $35 \times 35\text{-mm}^2$ field of view, 256×128 matrices, and one excitation for each phase encoding step. During MRI sessions, the spontaneously breathing animals were anesthetized with 1.5% isoflurane in 50% O_2 and 50% air.

2.3. Histochemistry

At nine days after Aβ42 and microglial injection, rats were perfused with cold fixative consisting of 4% paraformaldehyde in 100 mM phosphate buffer. Brain sections were cut into 20 μm thick slices with a

*Corresponding authors. Fax: +81 75 595 4796 (Y. Kitamura); +81 77 548 2402 (I. Tooyama).
E-mail addresses: yo-kita@mb.kyoto-phu.ac.jp (Y. Kitamura), kinchan@belle.shiga-med.ac.jp (I. Tooyama).

[1]These contributors both served as senior authors.

Abbreviations: Aβ, amyloid-β; AD, Alzheimer's disease; DAB, 3,3′-diaminobenzidine; ELISA, enzyme-linked immunosorbent assay; GFAP, glial fibrillary acidic protein; HVJ-E, hemagglutinating virus of Japan envelop; Iba1, ionized calcium binding adaptor molecule 1; MAP2, microtubule-associated protein-2; MRI, magnetic resonance imaging; PBS, phosphate-buffered saline; TBS, tris-buffered saline; TNF, tumor necrosis factor

0014-5793/$32.00
doi:10.1016/j.febslet.2007.01.009

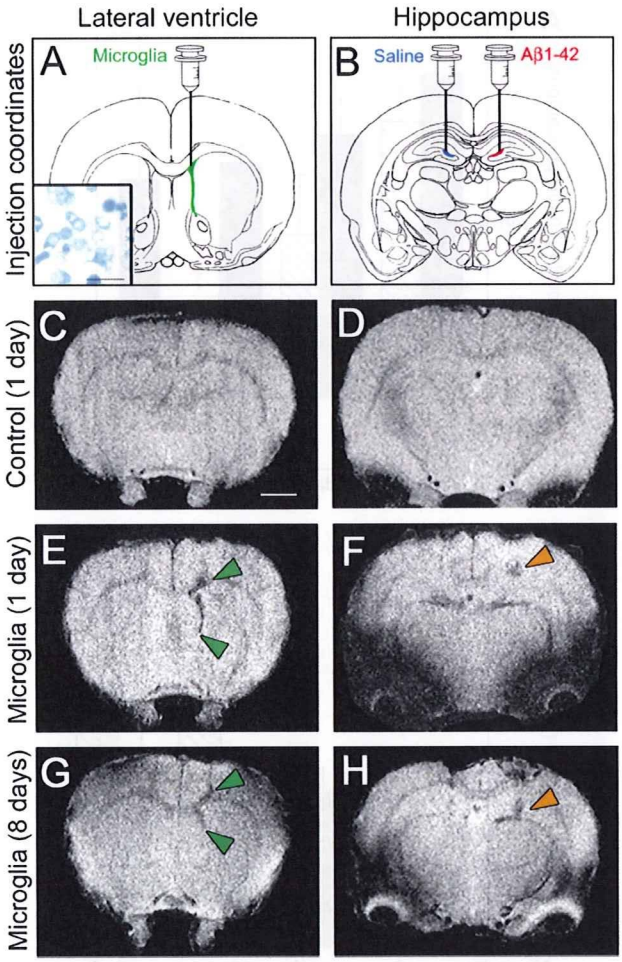

Fig. 1. Resovist-labeled rat microglia were transplanted (inset in A) into the left lateral ventricle (green in A) just after intra-hippocampal injections of saline (blue in B) and Aβ42 peptide (red in B). MR images in the control rat (non-microglial transplantation) at 1 day after Aβ injection are shown in (C) and (D). In MR images of rat grafted with microglia, the accumulation of exogenous microglia was detected as dark signals in the lateral ventricle (green arrowheads) and Aβ-injected site (orange arrowheads) at 1 day (E and F) and 8 days (G and H) after transplantation. Bars = 50 μm (inset in A), 2 mm (C–H).

cryostat. Serial hippocampal slices were incubated with primary antibodies, including anti-Aβ (clone 6E10, Chemicon), anti-ionized calcium binding adaptor molecule 1 (Iba1; Wako), and anti-CD68 (clone ED1, Serotec) antibodies. Other series were incubated with anti-microtubule-associated protein-2 (MAP2; Sigma), anti-glial fibrillary acidic protein (GFAP; Chemicon), and anti-oligodendrocytes (Chemicon) antibodies. Sections were followed by biotinylated secondary antibody, and then incubated with a Vectastain ABC elite kit (Vector). Subsequently, labeling was revealed with 3,3′-diaminobenzidine (DAB) with or without nickel ammonium. Counterstaining for ferric iron (Resovist) was examined by the Prussian blue method. In brief, sections were incubated for 30 min with 1% potassium ferrocyanide in 1% HCl at room temperature to stain iron particles blue.

2.4. ELISA

The amounts of Aβ42 and tumor necrosis factor (TNF)-α in hippocampi were measured by enzyme-linked immunosorbent assay (ELISA) kits for human Aβ42 and rat TNF-α (BioSource) according to the manufacturer's instructions, respectively. In brief, hippocampi on the Aβ-injected side were dissected and then the cytosolic fraction was extracted by 500 μl of tris-buffered saline (TBS) and the formic acid (FA) fraction extracted from the pellet by 500 μl of FA was prepared as described previously [10]. In our previous study, almost all Aβ42 was recovered from the FA fraction but little or none was found in the TBS fraction in Aβ-injected rats [11,12]; therefore, the amount of Aβ42 in the FA fractions was measured. Alternatively, expression levels of TNF-α were determined in TBS fractions as a marker for microglial activities. Results are given as the means ± standard error of the mean (S.E.M.). The statistical significance of differences was determined by analysis of variance (ANOVA), and the Bonferroni/Dunn test was carried out for post hoc comparisons.

3. Results

3.1. Exogenously transplanted microglia were detected on Aβ deposit by MRI

Transplanted microglia labeled with Resovist were traced by T_2^*-weighted MRI at a magnetic field of 7 T (Fig. 1C–H). In the control rat, which was an Aβ42-injected rat without microglial transplantation, there were no obvious changes in MR signals in both sides of lateral ventricles (Fig. 1C) and hippocampi (Fig. 1D). In the Aβ42-injected rat transplanted with Resovist-labeled microglia, a dark area indicating the decrease of MR signals was detected along with the left lateral ventricle at 1 day after transplantation (Fig. 1E). Furthermore, the dark area appeared in the Aβ42-injected left hippocampus (Fig. 1F). At eight days following transplantation, the dark area in the left lateral ventricle was decreased (Fig. 1G), while that in the left hippocampus was still clearly detected (Fig. 1H). These results suggest that iron particles phagocytosed by microglia reduce the MR signals and the dark areas may indicate the accumulation of exogenous microglia.

3.2. Accumulation of exogenous microglia on Aβ deposit was confirmed by histochemical analysis

The day after the MRI operation, the rat was sacrificed and then hippocampal sections were prepared. At the Aβ42 injection site (Fig. 2A), brown-colored microglia expressing Iba1 (Fig. 2B) or CD68 (phagocytic marker; Fig. 2C) infiltrated and some contained blue iron particles visualized by the Prussian blue method (Fig. 2D and E). We have reported recently that MAP2 immunoreactivity (neuronal marker) was moderately decreased by the neurotoxicity of Aβ42 in the Aβ42-injected rat [12]. In this study, we also found moderate loss of MAP2 immunoreactivity at the Aβ42 injection site (Fig. 2F). In addition, oligodendrocytes (Fig. 2G) surrounded the Aβ42 injection site and GFAP-immunoreactive astrocytes (Fig. 2H) were slightly activated in the region adjacent to the Aβ deposit. Blue iron was not co-localized with the immunoreactivity of MAP2 (Fig. 2I), oligodendrocytes (Fig. 2J), or GFAP (Fig. 2K); thus, iron-containing cells expressed a microglial marker. These results suggest that exogenously transplanted microglia in the lateral ventricle may migrate to the hippocampus and accumulate on the Aβ deposit together with endogenous microglia.

3.3. Microglial transplantation increased Aβ clearance and the expression level of TNF-α in rat hippocampus

Subsequently, we measured the amount of human Aβ42 injected into the rat hippocampus (Fig. 3A). Although the amount of Aβ42 was gradually reduced even in control rats, reduction was significantly increased by microglial transplantation at 7 and 14 days after the injection of Aβ42. Furthermore, we measured the expression levels of TNF-α, a

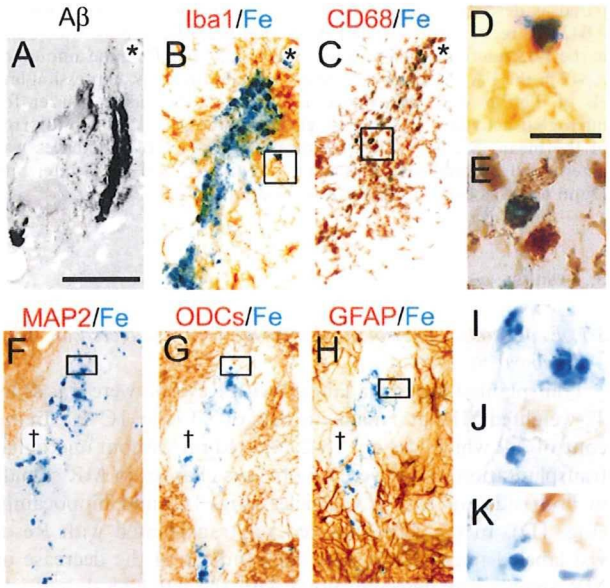

Fig. 2. The day after the MRI operation, rats were sacrificed and then fixed brain sections were prepared. One series of serial hippocampal sections in the Aβ-injected site was stained with antibodies against Aβ (A), Iba1 (marker for microglia; brown in B and D), and CD68 (phagocytic marker; brown in C and E). Another series was stained with antibodies against MAP2 (marker for neurons; brown in F and I), oligodendrocytes (ODCs; brown in G and J), and GFAP (marker for astrocytes; brown in H and K). Resovist was visualized by the Prussian blue method (blue particles in B–K). High magnifications of squares in B, C, F, G, and H are shown in D, E, I, J, and K, respectively. Scale bars = 100 μm (A–C and F–H), 20 μm (D, E and I–J). Asterisks and daggers indicate identical blood vessels in A–C and F–H, respectively.

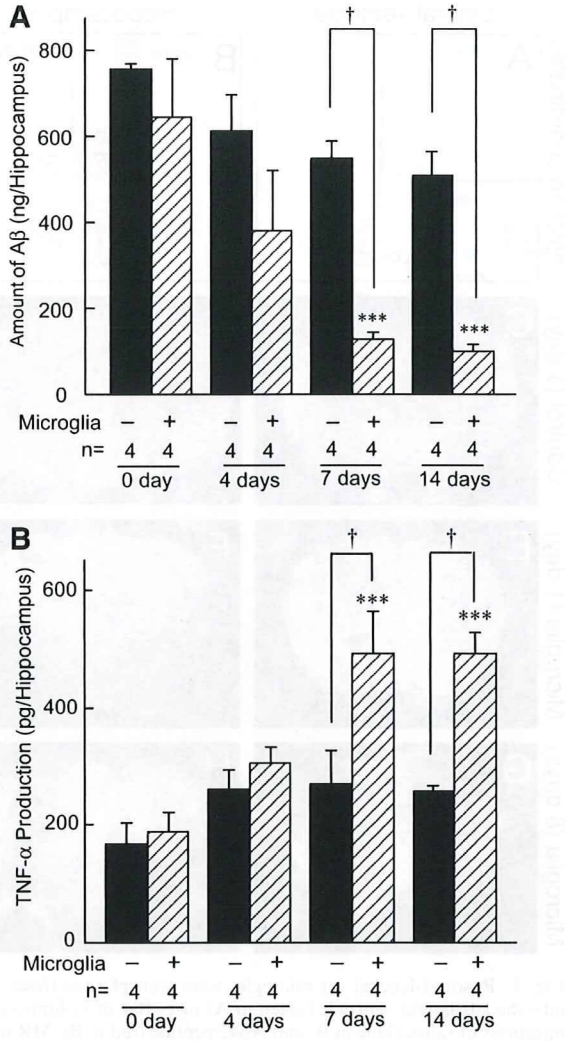

Fig. 3. Amounts of Aβ42 (A) and TNF-α (B) in rat hippocampus with (hatched column) or without (black column) microglial transplantation were measured by ELISA. $^{***}P < 0.001$ vs. the value in control rats at day 0. $^{\dagger}P < 0.05$ vs. value at the same time point. *n*: number of rats.

cytokine produced by microglia, as a marker of microglial activities (Fig. 3B). The amounts of TNF-α were slightly increased in control rats. At 7 and 14 days after the injection of Aβ42, the amount of TNF-α in rats transplanted with microglia was significantly higher than those in control rats. These results indicate that exogenous microglia accumulated on the Aβ deposit may retain its activities, such as phagocytic function and cytokine production.

4. Discussion

Previous reports demonstrated that microglia are able to phagocytose Aβ [4,13]. We also found that microglia markedly phagocytosed Aβ (see Supplemental information and Supplemental movie 1) and then degraded it by cathepsin D and/or insulin-degrading enzyme-like proteases in the in vitro study [14]. Neurons [15] and astrocytes [16] are also involved in Aβ clearance in in vivo brain. In the Aβ42-injected rat, moderate neuronal loss was induced and astrocytes were slightly activated in the region adjacent to the Aβ deposit, whereas endogenous microglia were accumulated on the Aβ deposit in our present and previous studies [12]. In addition, we have found regulatory factors of microglial Aβ phagocytosis in in vitro study, and the effects of these factors were well reflected by the Aβ clearance in the Aβ42-injected rat [11,12,14]. Thus, Aβ42-injected rats are a good model in the evaluation of microglial contribution to Aβ clearance in the in vivo brain. Here, microglial transplantation did not seem to obviously influence residential cells around the Aβ deposit, such as neurons, astrocytes, and endogenous microglia in morphological analysis by immunohistochemistry, while exogenous microglia markedly infiltrated the Aβ deposit. This infiltration may have continued through the experimental period because the dark area detected by MRI moved from the upper to middle and/or lower regions of the Aβ-injected hippocampus between 1 and 8 days. On the other hand, the dark area in the left lateral ventricle was decreased at 8 days compared to that at 1 day. Subsequently, lasting infiltration of exogenous microglia may be responsible for the significant increase of Aβ clearance and cytokine production after 7 days. Although we are not sure about the mechanisms for the recruitment of exogenous microglia in this study, we speculate that chemokines produced by endogenous microglia and/or astrocytes activated around the Aβ deposit are involved in this recruitment.

In the AD brain, microglial phagocytosis is suggested to work for Aβ clearance as shown in a case report of the human clinical trial of Aβ immunotherapy [17]. This observation is

supported by a report indicating positive correlations between the accumulation of reactive microglia and the reduction of senile plaques in an incomplete ischemic brain of a typical case of AD [18]. Microglial Aβ phagocytosis may have therapeutic potential for AD; however, the non-specific activation of microglia could alternatively cause harm as neuroinflammation [19]. Although further studies are required to confirm the microglial influence on neuronal viability, recent studies suggest that the signaling of $P2X_7$ receptors [20] and the fractalkine receptor [21] may play a key role in microglial neuroprotection and the attenuation of microglial neurotoxicity, respectively. Furthermore, several groups have recently demonstrated that bone marrow-derived cells are able to differentiate into functional microglia [22–24] and the implication of bone marrow-derived microglia in Aβ clearance is also suggested [25]. Thus, bone marrow cells may be a suitable source of microglial progenitors in clinical application. Additionally, previous studies have reported that intra-arterially injected microglia can migrate through an intact or injured blood–brain barrier to the brain parenchyma [26,27].

Here, we demonstrated the possible usefulness of exogenously transplanted microglia for the clearance of Aβ in the in vivo brain; however, further studies are needed before the clinical use. In future studies, the methodology will be required to trace exogenous microglia after transplantation. In this study, MRI is suggested to be one powerful tool as a non-invasive means of detecting transplanted microglia. We believe that investigations into microglia may provide a novel insight for AD therapy.

Acknowledgments: We thank Dr. Kato of Ishihara Sangyo Kaisha Ltd., for technical assistance with usage of the HVJ-E vector. This study was supported in part by the 21st COE and Open Research Programs; and grants-in-aid from the Ministry of Education, Culture, Sports, Science and Technology of Japan, the Ministry of Health, Labor and Welfare of Japan, the Japan Society for the Promotion of Science, the Takeda Science Foundation, the Kato Memorial Trust for Nambyo Research, the Smoking Research Foundation, and the Philip Morris USA Inc. and Philip Morris International.

Appendix A. Supplementary data

Supplementary data associated with this article can be found, in the online version, at doi:10.1016/j.febslet.2007.01.009.

References

[1] Hardy, J. and Selkoe, D.J. (2002) The amyloid hypothesis of Alzheimer's disease: progress and problems on the road to therapeutics. Science 297, 353–356.
[2] Akiyama, H. et al. (2000) Inflammation and Alzheimer's disease. Neurobiol. Aging 21, 383–421.
[3] Schenk, D. et al. (1999) Immunization with amyloid-beta attenuates Alzheimer-disease like pathology in the PDAPP mouse. Nature 400, 173–177.
[4] Bard, F. et al. (2000) Peripherally administered antibodies against amyloid-β peptide enter the central nervous system and reduce pathology in a mouse model of Alzheimer disease. Nat. Med. 6, 916–919.
[5] Janus, C. et al. (2000) Aβ peptide immunization reduces behavioral impairment and plaques in a model of Alzheimer's disease. Nature 408, 979–982.
[6] Morgan, D. et al. (2000) Aβ peptide vaccination prevents memory loss in an animal model of Alzheimer's disease. Nature 408, 982–985.
[7] Paxinos, G. and Watson, C. (2005) The Rat Brain in Stereotaxic Coordinates, 5th edn, Elsevier Academic Press, Burlington, San Diego, London.
[8] Kitamura, Y., Spleiss, O., Li, H., Taniguchi, T., Kimura, H., Nomura, Y. and Gebicke-Haerter, P.J. (2001) Lipopolysaccharide-induced switch between retinoid receptor (RXR) alpha and glucocorticoid attenuated response gene (GARG)-16 messenger RNAs in cultured rat microglia. J. Neurosci. Res. 64, 553–563.
[9] Toyoda, K., Tooyama, I., Kato, M., Sato, H., Morikawa, S., Hisa, Y. and Inubushi, T. (2004) Effective magnetic labeling of transplanted cells with HVJ-E for magnetic resonance imaging. Neuroreport 15, 589–593.
[10] Kawarabayashi, T., Younkin, L.H., Saido, T.C., Shoji, M., Ashe, K.H. and Younkin, S.G. (2001) Age-dependent changes in brain, CSF, and plasma amyloid β protein in the Tg2576 transgenic mouse model of Alzheimer's disease. J. Neurosci. 21, 372–381.
[11] Takata, K., Kitamura, Y., Tsuchiya, D., Kawasaki, T., Taniguchi, T. and Shimohama, S. (2003) Heat shock protein-90-induced microglial clearance of exogenous amyloid-beta1-42 in rat hippocampus in vivo. Neurosci. Lett. 344, 87–90.
[12] Takata, K., Kitamura, Y., Tsuchiya, D., Kawasaki, T., Taniguchi, T. and Shimohama, S. (2004) High mobility group box protein-1 inhibits microglial Abeta clearance and enhances Abeta neurotoxicity. J. Neurosci. Res. 78, 880–891.
[13] Rogers, J. and Lue, L.F. (2001) Microglial chemotaxis, activation, and phagocytosis of amyloid beta-peptide as linked phenomena in Alzheimer's disease. Neurochem. Int. 39, 333–340.
[14] Kakimura, J. et al. (2002) Microglial activation and β-amyloid clearance induced by exogenous heat-shock proteins. FASEB J. 16, 601–603.
[15] Iwata, N. et al. (2001) Metabolic regulation of brain Abeta by neprilysin. Science 292, 1550–1552.
[16] Wyss-Coray, T., Loike, J.D., Brionne, T.C., Lu, E., Anankov, R., Yan, F., Silverstein, S.C. and Husemann, J. (2003) Adult mouse astrocytes degrade amyloid-beta in vitro and in situ. Nat. Med. 9, 453–457.
[17] Nicoll, J.A., Wilkinson, D., Holmes, C., Steart, P., Markham, H. and Weller, R.O. (2003) Neuropathology of human Alzheimer disease after immunization with amyloid-β peptide: a case report. Nat. Med. 9, 448–452.
[18] Akiyama, H. and McGeer, P.L. (2004) Specificity of mechanisms for plaque removal after Aβ immunotherapy for Alzheimer disease. Nat. Med. 10, 117–118.
[19] McGeer, P.L. and McGeer, E.G. (2001) Inflammation, autotoxicity and Alzheimer disease. Neurobiol. Aging 22, 799–809.
[20] Suzuki, T., Hide, I., Ido, K., Kohsaka, S., Inoue, K. and Nakata, Y. (2004) Production and release of neuroprotective tumor necrosis factor by P2X7 receptor-activated microglia. J. Neurosci. 24, 1–7.
[21] Cardona, A.E. et al. (2006) Control of microglial neurotoxicity by the fractalkine receptor. Nat. Neurosci. 9, 917–924.
[22] Hess, D.C. et al. (2004) Hematopoietic origin of microglial and perivascular cells in brain. Exp. Neurol. 186, 134–144.
[23] Simard, A.R. and Rivest, S. (2004) Bone marrow stem cells have the ability to populate the entire central nervous system into fully differentiated parenchymal microglia. FASEB J. 18, 998–1000.
[24] Malm, T.M., Koistinaho, M., Parepalo, M., Vatanen, T., Ooka, A., Karlsson, S. and Koistinaho, J. (2005) Bone-marrow-derived cells contribute to the recruitment of microglial cells in response to beta-amyloid deposition in APP/PS1 double transgenic Alzheimer mice. Neurobiol. Dis. 18, 134–142.
[25] Simard, A.R., Soulet, D., Gowing, G., Julien, J.P. and Rivest, S. (2006) Bone marrow-derived microglia play a critical role in restricting senile plaque formation in Alzheimer's disease. Neuron 49, 489–502.
[26] Imai, F., Sawada, M., Suzuki, H., Kiya, N., Hayakawa, M., Nagatsu, T., Marunouchi, T. and Kanno, T. (1997) Migration activity of microglia and macrophages into rat brain. Neurosci. Lett. 237, 49–52.
[27] Imai. F., Suzuki. H., Oda, J., Ninomiya, T., Ono, K., Sano, H. and Sawada, M. (2006) Neuroprotective effect of exogenous microglia in global brain ischemia. J. Cereb. Blood Flow Metab. advance online publication 5 July 2006; doi:10.1038/sj.jcbfm.9600362.

Journal of Cerebral Blood Flow & Metabolism (2008) 28, 563–578

www.jcbfm.com

DJ-1 protects against neurodegeneration caused by focal cerebral ischemia and reperfusion in rats

Daijiro Yanagisawa[1], Yoshihisa Kitamura[1,9], Masatoshi Inden[1], Kazuyuki Takata[1], Takashi Taniguchi[1], Shigehiro Morikawa[2], Masahito Morita[2,3], Toshiro Inubushi[2], Ikuo Tooyama[4], Takahiro Taira[5], Sanae MM Iguchi-Ariga[6], Akinori Akaike[7] and Hiroyoshi Ariga[8,9]

[1]*Department of Neurobiology, 21st Century COE Program, Kyoto Pharmaceutical University, Kyoto, Japan;* [2]*Biomedical MR Science Research Center, Shiga University of Medical Science, Otsu, Japan;* [3]*PRESTO, Japan Science and Technology Agency, Kawaguchi, Japan;* [4]*Molecular Neuroscience Research Center, Shiga University of Medical Science, Otsu, Japan;* [5]*Department of Molecular Cell Biology, Interdisciplinary Graduate School of Medicine and Engineering, University of Yamanashi, Chuo, Japan;* [6]*Graduate School of Agriculture, Hokkaido University, Sapporo, Japan;* [7]*Department of Pharmacology, Graduate School of Pharmaceutical Sciences, Kyoto University, Kyoto, Japan;* [8]*Department of Molecular Biology, Graduate School of Pharmaceutical Sciences, Hokkaido University, Sapporo, Japan*

Reactive oxygen species (ROS) is massively produced in the brain after cerebral ischemia and reperfusion. It reacts strongly with cellular components, which has detrimental effects and leads to neuronal cell death. DJ-1, which was found to be the causative gene of familial Parkinson's disease PARK7, is a multifunction protein, which plays a key role in transcriptional regulation, and a molecular chaperone. In this study, we investigated the neuroprotective effect of DJ-1 against neurodegeneration caused by ischemia/reperfusion injury. Cerebral ischemia was induced in rats by 120 mins of middle cerebral artery occlusion (MCAO) using an intraluminal introduction method. The intrastriatal injection of recombinant glutathione *S*-transferase-tagged human DJ-1 (GST-DJ-1) markedly reduced infarct size in 2,3,5-triphenyltetrazolium chloride staining at 3 days after MCAO. In addition, we performed a noninvasive evaluation of ischemic size using magnetic resonance imaging and found a significant reduction of infarct size with the administration of GST-DJ-1. In GST-DJ-1-treated rats, behavioral dysfunction and nitrotyrosine formation were significantly inhibited. Furthermore, GST-DJ-1 markedly inhibited H_2O_2-mediated ROS production in SH-SY5Y cells. These results indicate that GST-DJ-1 exerts a neuroprotective effect by reducing ROS-mediated neuronal injury, suggesting that DJ-1 may be a useful therapeutic target for ischemic neurodegeneration.
Journal of Cerebral Blood Flow & Metabolism (2008) **28**, 563–578; doi:10.1038/sj.jcbfm.9600553; published online 19 September 2007

Keywords: DJ-1; focal cerebral ischemia; ischemia/reperfusion injury; neuroprotection; reactive oxygen species

Introduction

Cerebral ischemia occurs as a result of a local reduction or an arrest of blood supply and can lead to neuronal cell death in the ischemic region. The pathophysiologic mechanisms of the ischemia/reperfusion injury are complex. Neurons and glial cells are lethally damaged by several events such as periinfarct depolarization, which occur within hours after the onset of ischemia, and the production of reactive oxygen species (ROS), which occurs immediately after ischemia/reperfusion, is followed by more delayed postischemic inflammation and apoptosis, and these events are involved in the progression and expansion of brain injury (Hata

Correspondence: Dr Y Kitamura, Department of Neurobiology, 21st Century COE Program, Kyoto Pharmaceutical University, 5 Nakauchi-cho, Misasagi, Yamashina-ku, Kyoto 607-8414, Japan, E-mail: yo-kita@mb.kyoto-phu.ac.jp or Dr H Ariga, Department of Molecular Biology, Graduate School of Pharmaceutical Sciences, Hokkaido University, Kita-12, Nishi-6, Kita-ku, Sapporo 060-0812, Japan. E-mail: hiro@pharm.hokudai.ac.jp
[9]Senior authors
This study was supported in part by the 21st Century Center of Excellence (COE) and Open Research Programs; grants-in-aid from the Ministry of Education, Culture, Sports, Science and Technology of Japan; and by the Program for Promotion of Fundamental Studies in Health Sciences of the National Institute of Biomedical Innovation (NIBIO) in Japan.
Received 12 March 2007; revised 10 August 2007; accepted 15 August 2007; published online 19 September 2007

et al, 2000; Peters *et al*, 1998). This burst of ROS is involved in direct cytotoxic effects, including protein and lipid peroxidation, oxidative DNA damage, and postischemic inflammatory injury, through redox-mediated signaling pathways (Andersen, 2004; Margaill *et al*, 2005). The oxidation of proteins can have wide-ranging damaging effects such as disruption of the active sites of enzymes or alteration of the conformation of structural proteins. Oxidative modification of susceptible unsaturated fatty acids can result in the generation of lipid peroxides, which can further oxidize nearby unsaturated fatty acids in a chain-reaction event. This event can disrupt both the plasma membrane and membranes that are components of cellular organelles, such as mitochondria. Thus, the components of ROS are believed to make a contribution to neuronal loss after ischemia/reperfusion (Andersen, 2004; Margaill *et al*, 2005). Therefore, the control of ROS production is important for achieving neuroprotection against ischemia/reperfusion injury.

DJ-1 was originally identified as a novel oncogene in collaboration with activated small G-protein *ras* (Nagakubo *et al*, 1997) and it was later found to be the causative gene of familial Parkinson's disease PARK7 (Bonifati *et al*, 2003). DJ-1 is a multifunction protein, which is involved in transcriptional regulation and acts as a molecular chaperone (Niki *et al*, 2003; Shendelman *et al*, 2004; Shinbo *et al*, 2005; Takahashi *et al*, 2001). X-ray crystallographic and biologic analyses have shown that DJ-1 forms a homodimer. Furthermore, these analyses have also shown that the L166P mutation of DJ-1, which was first found in a PARK7 patient (Bonifati *et al*, 2003), disrupts dimer formation, resulting in a loss of function (Honbou *et al*, 2003; Huai *et al*, 2003; Inden *et al*, 2006; Tao and Tong, 2003; Wilson *et al*, 2003). It has been reported that the protein level of DJ-1 increased on exposure to oxidative stress (Jin *et al*, 2005; Mitsumoto *et al*, 2001). Furthermore, DJ-1 is directly oxidized by free radicals predominantly on the cysteine residue at amino-acid number 106 (Cys106) and it showed a shift in the isoelectric point (p*I*) from 6.2 to 5.8 (Canet-Aviles *et al*, 2004; Kinumi *et al*, 2004; Mitsumoto *et al*, 2001; Taira *et al*, 2004). However, recent studies using DJ-1-deficient mice have shown that loss of the *DJ-1* gene resulted in abrogation of dopamine receptor activity and sensitization of cells against oxidative stress, suggesting that loss of function of DJ-1 is correlated with pathogenesis of Parkinson's disease (Chen *et al*, 2005; Goldberg *et al*, 2005; Kim *et al*, 2005). However, DJ-1 function on brain ischemia-induced neurodegeneration is still unknown.

In this study, to evaluate the neuroprotective effect of DJ-1 against ischemia/reperfusion injury, we performed the intrastriatal injection of recombinant human DJ-1 protein in rats that had been subjected to middle cerebral artery occlusion (MCAO) and reperfusion. We then investigated its effects on infarct size, neuronal survival, and behavioral outcome. Moreover, we also examined the effects of DJ-1 on ROS-mediated oxidative stress in SH-SY5Y cells.

Materials and methods

Preparation of Recombinant Human DJ-1 Protein and Anti-DJ-1 Antibody

Recombinant glutathione *S*-transferase (GST)-tagged human DJ-1 protein (GST-DJ-1) was used throughout the present experiments. Recombinant proteins such as GST-DJ-1 and GST-tagged L166P-mutant human DJ-1 (GST-L166P-DJ-1) were expressed in and purified from *Escherichia coli* as described previously (Nagakubo *et al*, 1997; Takahashi *et al*, 2001). The preparation and specificity of a rabbit polyclonal or a mouse monoclonal anti-human DJ-1 antibody have been described previously (Inden *et al*, 2006; Nagakubo *et al*, 1997; Takahashi *et al*, 2001; and the specificity in this study was shown in Supplementary Figure S1).

Animals

Wistar rats were purchased from Japan SLC Inc. (Hamamatsu, Japan). The animals were acclimated to and maintained at 23°C under a 12-h light/dark cycle (light from 0800 to 2000 hours). Rats were housed in standard laboratory cages and had free access to food and water throughout the study period. All animal experiments were performed in accordance with the National Institutes of Health Guide for the Care and Use of Laboratory Animals, and the protocols were approved by the Committee for Animal Research at Kyoto Pharmaceutical University.

Rat Model of Focal Ischemia

Male Wistar rats weighing 260 to 300 g were used in this study. Focal cerebral ischemia was induced by the intraluminal introduction of a nylon thread (Nagasawa and Kogure, 1989) as described previously (Kitamura *et al*, 2005). Briefly, animals were anesthetized with 4% halothane (Takeda Pharmaceutical, Osaka, Japan) and maintained on 1.5% halothane using a face mask. After a midline neck incision was made, 20 mm of 4-0 nylon thread, with its tip rounded by heating and coated with silicon (Xantopren M; Heraeus Kulzer, Hanau, Germany), was inserted into the left internal carotid artery as far as the proximal end using a globular stopper. The origin of the middle cerebral artery was then occluded by a silicon-coated embolus. Anesthesia was discontinued, and the development of right hemiparesis with upper limb dominance was used as a criterion for ischemic insult. After 120 mins of MCAO, the embolus was withdrawn to allow reperfusion of the ischemic region through the anterior and posterior communicating arteries. Body temperature was maintained at 37 to 37.5°C with a heating pad and lamp during surgery. In the sham operation, a midline neck incision was made to expose the arteries, but the nylon thread was not inserted into the carotid artery.

Administration of Glutathione *S*-Transferase-Tagged Human DJ-1

For stereotaxic microinjection, rats were anesthetized (sodium pentobarbital; 50 mg/kg, intraperitoneally, Abbott Laboratories, North Chicago, IL, USA) and immobilized in a Kopf stereotaxic frame. Subsequently, rats were injected with GST (320 pmol), GST-DJ-1 (4, 40, 160, or 320 pmol), or phosphate-buffered saline (PBS) as the vehicle control in a final volume of 4 μL of PBS at 110 mins after the onset of MCAO (10 mins before reperfusion). To investigate the time window of efficacy, we injected GST-DJ-1 (320 pmol) at 60, 110, 180, and 300 mins after the onset of MCAO. The intrastriatal injection coordinates (1.0 mm anterior, 4.0 mm left lateral, 5.0 mm ventral from the bregma) were taken from a rat brain atlas (Paxinos and Watson, 2005). Injection was given by a motor-driven 10-μL Hamilton syringe using a 26-gauge needle. The infusion rate was 1 μL/min, and the injection cannula was kept in place for a further 5 mins after the injection.

Measurement of Infarct Size

At 3 days after MCAO, the brains were removed and cut into 2-mm-thick coronal sections. These sections were immersed in a 2% solution of 2,3,5-triphenyltetrazolium chloride (TTC; Wako Pure Chemical Industries, Osaka, Japan) in saline at 37°C for 20 mins and then fixed in 4% paraformaldehyde in 100 mmol/L phosphate buffer at 4°C. For quantification of infarct size, the brain sections were scanned using a camera (KY-F55MD; Victor, Tokyo, Japan), and the infarct size was then analyzed by computerized image analysis (WinRoof; Mitani, Fukui, Japan). Briefly, the infarct area in each section was calculated by subtracting the area of the normally stained ipsilateral hemisphere from the area of the contralateral hemisphere to reduce errors because of cerebral edema (Lin *et al*, 1993; Swanson *et al*, 1989). The infarct volume was calculated by multiplying the sum of the infarct areas by the distance between the sections.

Magnetic Resonance Imaging

Rats were sham-operated or operated on the MCAO and then received an intrastriatal injection with PBS (a vehicle control) or GST-DJ-1 (320 pmol) at 110 mins after the onset of MCAO (10 mins before reperfusion). After 7 days, magnetic resonance (MR) images of these rat heads were acquired with a 7 T Unity Inova MR scanner (Varian, Palo Alto, CA, USA). A T2-weighted MR sequence was used with acquisition parameters of 2,000 ms repetition time, 40 ms echo time, 35×35 mm^2 field of view, 1-mm slice thickness (total 24 slices) and 256×128 matrices. During the MR sessions, spontaneously breathing animals were anesthetized with 1.5% isoflurane in 50% O_2 and 50% air.

The infarct area was calculated from T2-weighted MR images using imaging software (WinRoof), as described above. For each slice, areas of high intensity in T2-weighted MR images were marked as ischemic lesion areas, and the infarct volume was calculated by taking slice thickness (1 mm/slice) into account.

Neurologic Evaluation

Neurologic deficits were assessed at 30 mins after the onset of MCAO (80 mins before injection of PBS, GST, or GST-DJ-1), and subsequently every day until the rats were killed at 7 days after MCAO. Neurologic findings were graded as severe, moderate, mild, or absent on a 4-point scale, according to the method described by Bederson *et al* (1986); a grade 3 (severe) neurologic deficit indicates reduced resistance to lateral pushing toward the right side and forelimb flexion with consistent circling toward the paretic side; a grade 2 (moderate) neurologic deficit indicates reduced resistance to lateral pushing toward the right side and forelimb flexion but without circling movement; a grade 1 (mild) neurologic deficit indicates any amount of consistent forelimb flexion but no other abnormality; and grade 0 indicates no observable neurologic deficit. In this study, the protection against ischemia-induced neurologic deficits was evaluated by this method, similar to previous studies (Gao *et al* 2005; Suzuki *et al*, 2005).

Rota-rod Test

Spontaneous motor activity was measured using the rota-rod treadmill for rats (accelerating model 7750; Ugo Basile, Varese, Italy), and the accelerating rotor mode was used (10 speeds from 4 to 40 r.p.m. for 5 mins). The interval from when the animal mounted the rod to when it fell off was recorded as the performance time (Kitamura *et al*, 2005). The animals were trained for five trials per day for 2 days before MCAO to obtain stable baseline values. The mean duration on the rod was recorded with five trials at 1 day before surgery. Performance on the rota-rod test was measured five times a day at 2 and 5 days after MCAO, and these data are presented as the mean duration on the rod. Subsequently, time-dependent change in the percentage (%) of walking rats on the rotating rod was calculated by the Kaplan–Meier method.

Methamphetamine-Induced Rotation Test

At 6 days after MCAO, the methamphetamine-induced rotation test was assessed in rotometer bowls as described previously (Inden *et al*, 2006; Kitamura *et al*, 2005). Briefly, the total number of full-turn rotations in the ipsilateral direction was counted for 60 mins after the intraperitoneal administration of methamphetamine (2.5 mg/kg; Dainippon Pharmaceutical, Osaka, Japan), which stimulates dopamine release on the intact right side and induces marked ipsilateral circling in animals with stroke.

Immunohistochemistry

The animals were perfused through the aorta with 150 mL of 10 mmol/L PBS, followed by 300 mL of a cold fixative consisting of 4% paraformaldehyde in 100 mmol/L phosphate buffer under deep anesthesia with sodium pentobarbital (50 mg/kg, intraperitoneally). After perfusion, the

brains were quickly removed and postfixed for 2 days with 4% paraformaldehyde in 100 mmol/L phosphate buffer and then transferred to 15% sucrose solution in 100 mmol/L phosphate buffer containing 0.1% sodium azide at 4°C. The brain pieces were cut 20 μm thick using a cryostat and collected in 100 mmol/L PBS containing 0.3% Triton X-100. The free-floating sections were treated with 0.3% hydrogen peroxide in PBS containing 0.3% Triton X-100 to eliminate endogenous peroxidase activity. After several washes, the sections were incubated for 3 days at 4°C with the following primary antibodies: mouse monoclonal antibodies against DJ-1 (dilution, 1:10,000), microtubule-associated protein-2 (MAP2) (1:3,000; Sigma, St Louis, MO, USA), and tyrosine hydroxylase (TH) (1:3,000; Sigma); rabbit polyclonal antibodies against GST (1:10,000; Cell Signaling Technology, Danvers, MA, USA); and nitrotyrosine (1:500; Chemicon International, Temecula, CA, USA). After several washes, the sections were incubated with biotinylated antibodies against mouse or rabbit IgG (1:2,000; Vector Laboratories, Burlingame, CA, USA) as appropriate for 2 h at room temperature. The sections were then incubated with avidin peroxidase (1:4,000; Vectastatin ABC Elite kit, Vector Laboratories) for 1 h at room temperature. All of the sections were washed several times with PBS containing 0.3% Triton X-100 between each incubation, and labeling was then revealed by 3,3′-diaminobenzidine (Dojindo Laboratories, Kumamoto, Japan), with nickel ammonium, which yielded a dark blue color.

For the semiquantitative analysis of GST-immunoreactive areas, the immunostained sections at +4, +3, +2, +1, ±0, −1, and −2 mm anterior–posterior from the bregma were also scanned using a camera, and these immunoreactive areas were measured by computerized image analysis (WinRoof).

To evaluate the level of oxidative and nitrosative stress, the sections that had been immunostained with anti-nitrotyrosine antibody at +1 mm anterior from the bregma were scanned using a camera. The number of nitrotyrosine-immunopositive cells was counted in a predefined area (2.015 mm^2) within the boundary zones of the ischemic core in the cerebral cortex and the striatum and in the ischemic core in the striatum using computerized image analysis (WinRoof).

Double-Immunofluorescence Staining

For double-immunofluorescence staining, the sections were simultaneously incubated for 3 days at 4°C with the following primary antibodies: mouse monoclonal antibodies against neuronal nuclei (NeuN, 1:5,000; Chemicon International), glial fibrillary acidic protein (1:3,000; Chemicon International), and CD11b (1:500; Serotec); and a rabbit polyclonal anti-GST antibody (1:5,000). The primary antibodies were detected with anti-mouse IgG antibody conjugated with Alexa Fluor 488 and a anti-rabbit IgG antibody conjugated with Alexa Fluor 546 (1:500; Molecular Probes, Eugene, OR, USA) for 2 h at room temperature. In addition, the sections were incubated with Hoechst 33342 (Molecular Probes) for 15 mins at room temperature. Fluorescence was then detected using a laser scanning confocal microscope (LSM410; Carl Zeiss, Jena, Germany)

Establishment of DJ-1-Knockdown Cell Line

The human neuroblastoma cell line SH-SY5Y was cultured in Dulbecco's modified Eagle's medium supplemented with 10% (v/v) fetal calf serum, 50 μg/mL penicillin, and 100 μg/mL streptomycin, and kept at 37°C in humidified 5% CO_2/95% air.

We established DJ-1-knockdown SH-SY5Y cell line by essentially similar method in mouse Flp-In3T3 cells (Takahashi-Niki *et al*, 2004). In brief, the nucleotide sequence of the upper strand of the oligonucleotide used for construction of an siRNA vector targeting human DJ-1 gene is 5′-GGATCCCGTCAAGGCTGGCATCAGGACAATT GATATCCGTTGTCCTGATGCCAGCCTTGATTTTTTCCAA AAGCTT-3′. After annealing oligonucleotides corresponding to the upper and lower strands of DNA, they were inserted into *Bam*HI–*Hin*dIII sites of pRNA-U6.1/Neo. These plasmids were transfected into SH-SY5Y cells by the calcium phosphate precipitation method, and the cells were cultured in RPMI-1640 medium in the presence of 400 μg/mL G418 for 14 days. The cells that were resistant to the drug were then selected and the intrinsic expression of DJ-1 was checked by western blotting with an anti-human DJ-1 antibody.

6-carboxy-2′,7′-Dichlorodihydrofluorescein Diacetate Di(acetoxymethyl) Ester Staining

To detect H_2O_2-induced ROS production, we used a redox-sensitive dye, 6-carboxy-2′,7′-dichlorodihydrofluorescein diacetate di(acetoxymethyl) ester (Molecular Probes) (Kitamura *et al*, 1998). 6-Carboxy-2′,7′-dichlorodihydrofluorescein diacetate di(acetoxymethyl) ester is readily taken up by cells. When it reacts with ROS, it is converted into 6-carboxy-2′,7′-dichlorodihydrofluorescence (C-DCF), and subsequently illuminates at an excitation wavelength of 488 nm. After the SH-SY5Y cells were prepared in uncoated glass-bottomed microwells (inner diameter, 18 mm), 6-carboxy-2′,7′-dichlorodihydrofluorescein diacetate di(acetoxymethyl) ester was added to the cell culture to a final concentration of 2 μmol/L for 10 mins at 37°C. After two rinses with a serum-free medium, the fluorescence intensity of C-DCF was scanned under a confocal microscope (LSM410). As illumination at an excitation wavelength of 488 nm causes increased fluorescence due to oxidation of this dye (Kitamura *et al*, 1998), each field was exposed to light for exactly the same amount of time. Fluorescence intensity was quantified by computerized image analysis (WinRoof).

Measurement of Cell Viability

To evaluate cell viability, we performed a 3-(4,5-dimethyl-2-thiazolyl)-2,5-diphenyltetrazolium bromide (MTT; Dojindo Laboratories) assay as an index of surviving cells. In living cells, MTT is converted to formazan, which has a

specific absorption maximum. SH-SY5Y cells, in which endogenous DJ-1 expression was normal or knocked down by an siRNA vector, were seeded at 3×10^4 cells/well in a 96-microwell plate and treated with 50 or 100 μmol/L H_2O_2 at 24 h after plating. At 24 h after treatment, the culture medium was changed to a medium containing 5 mg/mL MTT, and the cells were incubated for an additional 4 h. They were then mixed thoroughly with an equal volume of isopropanol/0.04 mol/L HCl and sonicated to dissolve formazan completely. Absorbance was then measured at 570 nm with a microplate reader (Bio-Rad Laboratories, Hercules, CA, USA).

Western Blot Analysis

Cell lysates were diluted with Laemmli's sample buffer and subjected to sodium dodecyl sulfate–polyacrylamide gel electrophoresis (15% polyacrylamide gel), and immunoblotting was then carried out using antibodies against human DJ-1 (1:5,000) and β-actin (1:10,000). For semi-quantitative analysis, the bands of these proteins on radiographic films were scanned with a charge-coupled device color scanner (DuoScan; AGFA, Leverkusen, Germany), and then analyzed. Densitometric analysis was performed using the public domain program NIH Image 1.56 (written by Wayne Rasband at the US National Institutes of Health and available from the Internet through anonymous FTP from zippy.nimh. nih.gov).

Statistical Analysis

Results are given as the mean $\pm$ s.e.m. The significance of differences was determined by Student's *t*-test for single comparisons and an analysis of variance (ANOVA) and *post hoc* Bonferroni/Dunn test for multiple comparisons (StatView; Abacus Concepts, Berkeley, CA, USA). In neurologic evaluation, the significance of differences was determined by the nonparametric Kruskal–Wallis test followed by *post hoc* Scheffe's test for multiple comparisons. In rota-rod test, time-dependent change in the percentage (%) of walking rats on the rotating rod (walking survivor) was calculated by the Kaplan–Meier method. The statistical significance of differences was analyzed by the log-rank (Mantel-Cox) test.

Results

Effect of Recombinant Glutathione *S*-Transferase-Tagged Human DJ-1 on Infarct Size

In a preliminary experiment, to detect the human DJ-1 protein, which was exogenously injected into the rat striatum, we compared immunohistochemical staining between anti-human DJ-1 antibody and anti-GST antibody. Anti-human DJ-1 antibody induced nonspecific staining with moderate intensity of some neural staining, but this antibody did not recognize rat DJ-1 by immunoblotting (Supplementary Figure S1). While anti-GST antibody specifically reacted with GST-DJ-1 without nonspecific staining in the rat brain (Supplementary Figure S1). As we reported previously antioxidative and cellular protective effects of GST-free DJ-1 (Taira *et al*, 2004) and GST-DJ-1 (Inden *et al*, 2006), we basically consider that GST-DJ-1 has almost the same properties as GST-free DJ-1. On the basis of these observations, we used GST-DJ-1 in this study, while we utilized PBS and GST (320 pmol) as vehicle controls, as GST-DJ-1 (4 to 320 pmol) was injected with PBS.

At 3 days after MCAO, although a regional loss of TTC staining was observed in the ipsilateral cerebral cortex and the striatum in PBS- and GST-injected rats, the area of TTC staining lost was smaller with the administration of GST-DJ-1 at 110 mins after the onset of MCAO (10 mins before reperfusion; Figure 1A). In the quantitative analysis, the infarct area was reduced in a dose-dependent manner by the administration of GST-DJ-1, and the total infarct volume was significantly reduced by the administration of GST-DJ-1 at 160 and 320 pmol, compared with PBS- and GST-injected rats (Figures 1B and 1C).

The delayed administration of GST-DJ-1 (320 pmol) significantly reduced the infarct volume when the injection was performed at 60 and 110 mins after the onset of MCAO. However, this effect was lost when the injection was delayed to 180 mins (Figures 1D and 1E). At that time, although the total infarct volume did not significantly change, the infarct area at the level of -1 mm from the bregma was significantly smaller with the administration of GST-DJ-1 at 180 mins after the onset of MCAO (Figure 1D).

Quantification of Infarct Lesion Using Magnetic Resonance Imaging

We further investigated the neuroprotective effect of GST-DJ-1 using MR imaging. In sham-operated rats, which had been injected with PBS and GST-DJ-1 (320 pmol), any difference of MR signal between PBS- and GST-DJ-1-injected rats was not detected on T2-weighted MR images at 7 days after the injection (Figure 2A). In ischemic rats, which had been injected with PBS at 110 mins after the onset of MCAO, the infarct lesion, as represented by an area of hyperintensity (white), was markedly observed in the ipsilateral cortex and striatum at 7 days after MCAO (Figure 2B and Supplementary Movie S2). In contrast, the infarct lesion was markedly smaller in ischemic rats, which had been injected with GST-DJ-1 (320 pmol) at 110 mins after the onset of MCAO (Figure 2B and Supplementary Movie S2). In the quantitative analysis, GST-DJ-1-injected rats showed a significant reduction of infarct size, compared with PBS-injected rats (Figures 2C and 2D).

Effect of Glutathione *S*-Transferase-Tagged Human DJ-1 on Ischemia-Induced Behavioral Dysfunction

To evaluate the effect of GST-DJ-1 on behavior, the animals were subjected to sham operation or MCAO,

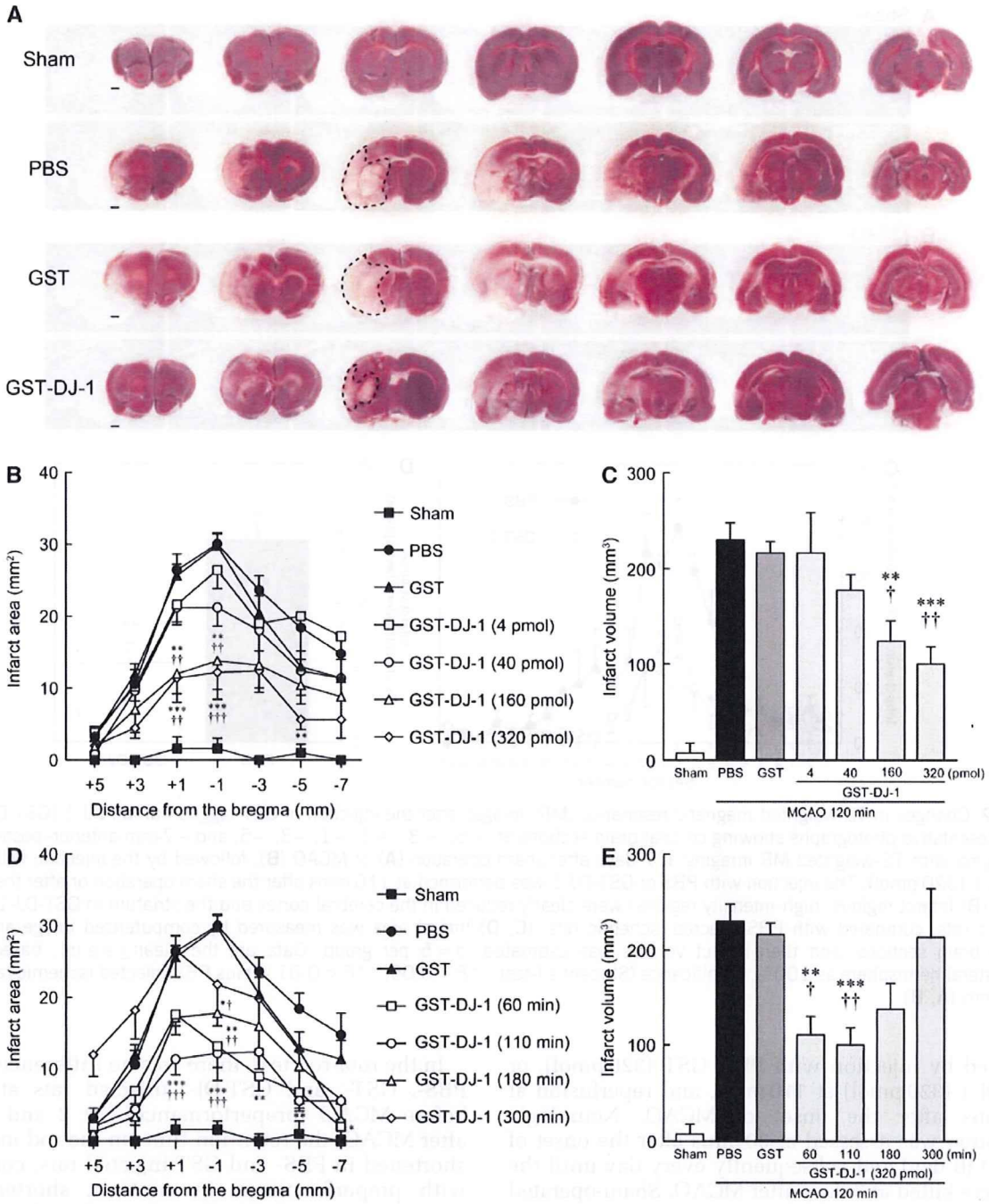

Figure 1 Glutathione *S*-transferase-tagged human DJ-1 (GST-DJ-1) reduces infarct size after cerebral ischemia and reperfusion. (**A**) Representative photographs showing coronal brain sections at + 5, + 3, + 1, −1, −3, −5, and −7 mm anterior–posterior from the bregma with TTC staining at 3 days after MCAO in sham-operated rats and middle cerebral artery-ischemic rats injected with phosphate-buffered saline (PBS), Glutathione *S*-transferase (GST, 320 pmol), which is as controls or GST-DJ-1 (320 pmol) at 110 mins after the onset of MCAO (10 mins before reperfusion). (**B**, **C**) Dose-dependent protection by GST-DJ-1. Phosphate-buffered saline ($n = 8$), GST (320 pmol, $n = 7$), or GST-DJ-1 at a dose of 4 ($n = 4$), 40 ($n = 6$), 160 ($n = 6$), or 320 pmol ($n = 7$) was injected at 110 mins after the onset of MCAO, and the infarct area (**B**) and volume (**C**) were measured on the basis of the regional loss of TTC staining (as indicated in the brain section in (**A**)). The sham group ($n = 4$) was subjected to a sham operation followed by PBS injection. (**D**, **E**) Time window of the efficacy of GST-DJ-1. Glutathione *S*-transferase-tagged human DJ-1 (320 pmol) was injected at 60 ($n = 6$), 110 ($n = 7$), 180 ($n = 4$), or 300 mins ($n = 4$) after the onset of MCAO, and infarct area (**D**) and volume (**E**) were measured. Data are the mean ± s.e.m. Significance (Bonferroni/Dunn *post hoc* comparisons after ANOVA): $^{*}P < 0.05$, $^{**}P < 0.01$, $^{***}P < 0.001$ versus PBS-injected rats. $^{\dagger}P < 0.05$, $^{\dagger\dagger}P < 0.01$, $^{\dagger\dagger\dagger}P < 0.001$ versus GST-injected rats. Scale bar: 1 mm (**A**).

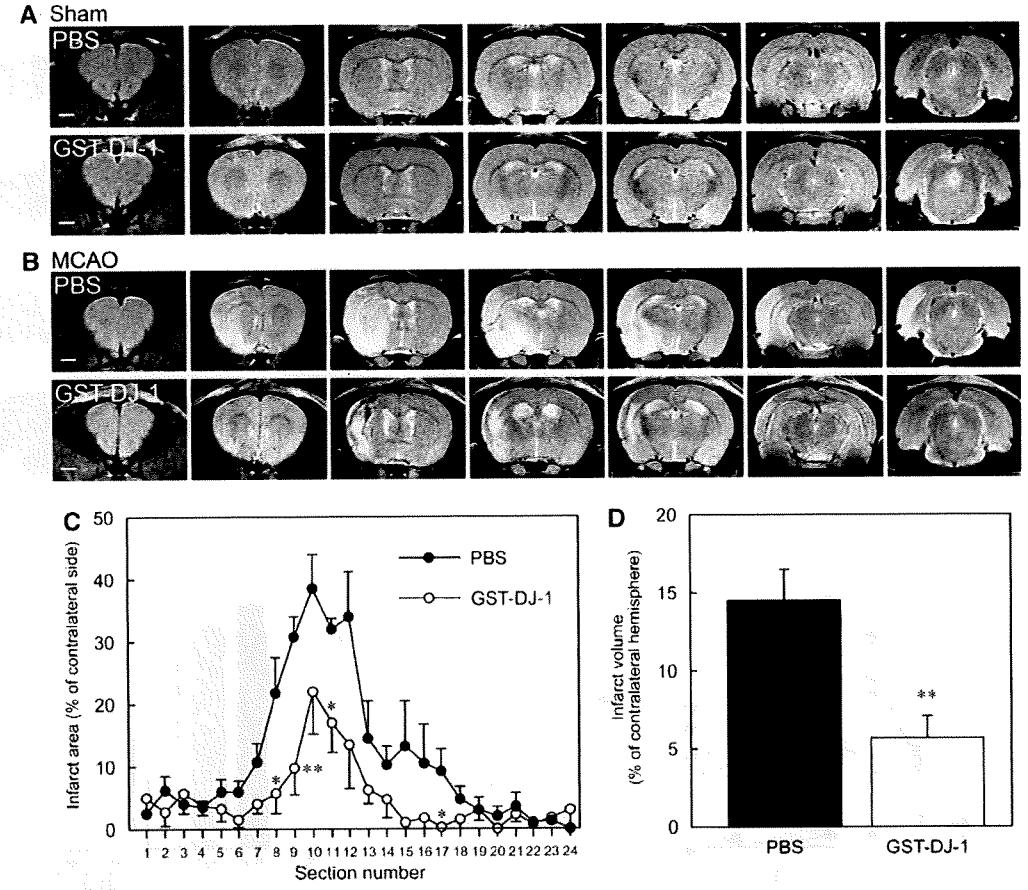

Figure 2 Changes in T2-weighted magnetic resonance (MR) images after the injection of GST-tagged human DJ-1 (GST-DJ-1). (**A**, **B**) Representative photographs showing coronal brain sections at +5, +3, +1, −1, −3, −5, and −7 mm anterior–posterior from the bregma with T2-weighted MR imaging at 7 days after sham operation (**A**) or MCAO (**B**), followed by the injection with PBS or GST-DJ-1 (320 pmol). The injection with PBS or GST-DJ-1 was performed at 110 mins after the sham operation or after the onset of MCAO. (**B**) Infarct regions (high-intensity regions) were clearly reduced in the cerebral cortex and the striatum in GST-DJ-1-injected ischemic rats, compared with PBS-injected ischemic rats. (**C**, **D**) Infarct area was measured by computerized image analysis in coronal brain sections, and then infarct volume was estimated. $n = 5$ per group. Data are the mean±s.e.m., based on the contralateral hemisphere as 100%. Significance (Student's *t*-test): $^{*}P < 0.05$, $^{**}P < 0.01$ versus PBS-injected ischemic rats. Scale bar: 2 mm (**A**, **B**).

followed by injection with PBS, GST (320 pmol), or GST-DJ-1 (320 pmol) at 110 mins, and reperfusion at 120 mins after the onset of MCAO. Neurologic evaluation was assessed at 30 mins after the onset of MCAO (0 day) and subsequently every day until the rats were killed at 7 days after MCAO. Sham-operated rats showed no abnormal behavior at any time points. At 30 mins after the onset of MCAO (80 mins before injection of PBS, GST, or GST-DJ-1), ischemic rats caused severe neurologic deficits and did not show any difference in neurologic score among these rats (at 0 day). Subsequently, the neurologic grade in PBS- and GST-injected ischemic rats gradually decreased. However, GST-DJ-1-injected rats showed more improvement of neurologic grade than PBS- and GST-injected rats. In brief, neurologic deficits were significantly recovered at 3, 4, 5, and 6 days by GST-DJ-1 injection, in comparison with those by injection of PBS or GST (Figure 3A).

In the rota-rod test, there was no difference among PBS-, GST-, and GST-DJ-1-injected rats at 1 day before MCAO (preperformance). At 2 and 5 days after MCAO, the retention time on the rod markedly shortened in PBS- and GST-injected rats, compared with preperformance. In contrast, shortening of retention time was significantly inhibited by administration of GST-DJ-1 (Figure 3B). In addition, the population of ischemic rats, which walked for a long time on the accelerating rotating rod, significantly increased by GST-DJ-1 injection at 2 and 5 days after MCAO, in comparison with that by PBS injection ($P = 0.0067$ and $P = 0.0117$ by the log-rank test) or GST injection ($P = 0.0286$ and $P = 0.0027$), respectively (Figure 3C).

We further examined methamphetamine-induced rotation asymmetry. In PBS- or GST-injected rats, the total number of rotations every 5 mins gradually increased until 30 mins after methamphetamine

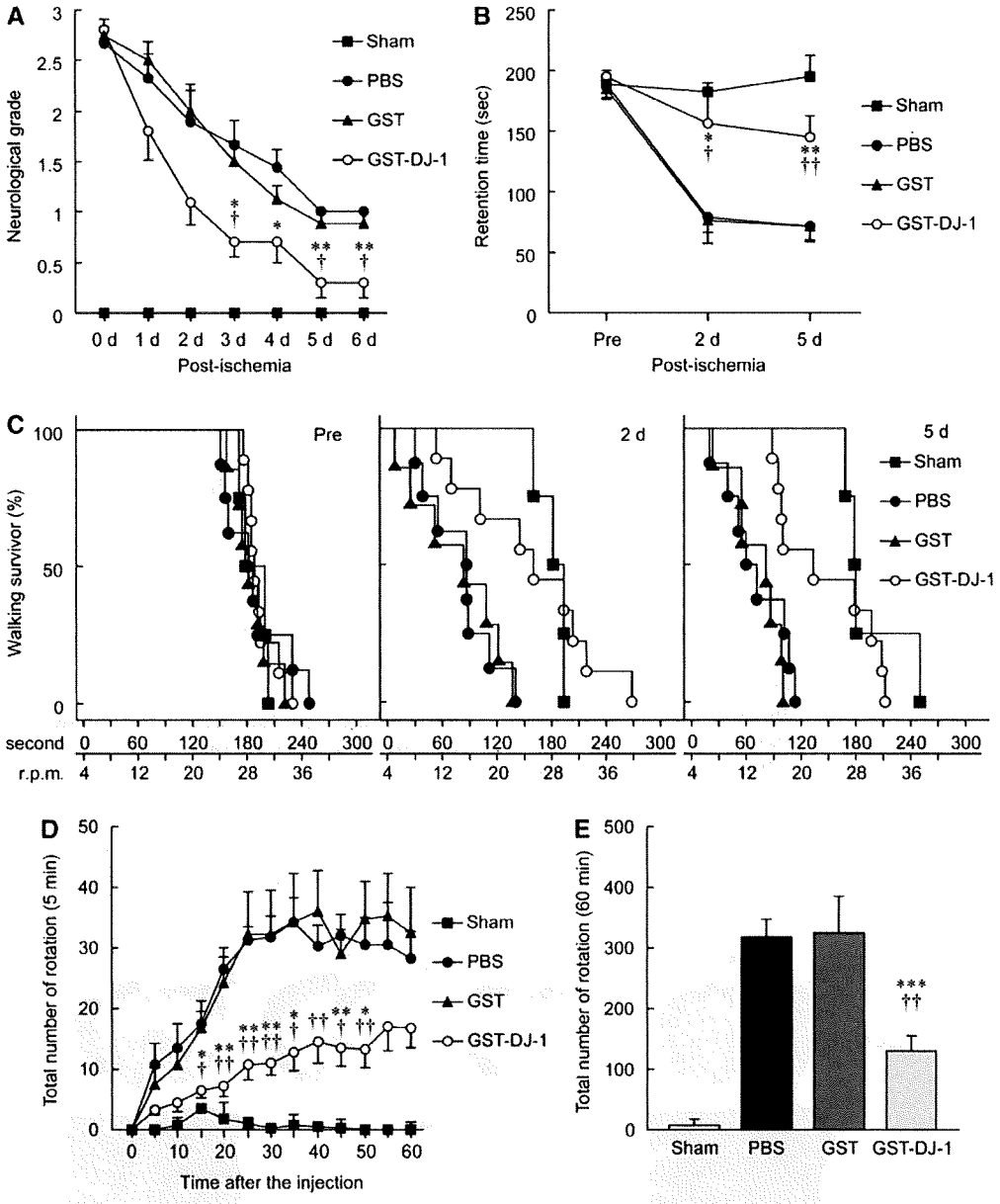

Figure 3 Effect of GST-tagged human DJ-1 (GST-DJ-1) on behavioral dysfunction induced by cerebral ischemia and reperfusion. Rats were subjected to MCAO followed by injection with PBS ($n = 8$), GST (320 pmol; $n = 7$), or GST-DJ-1 (320 pmol; $n = 9$) at 110 mins after the onset of MCAO. (**A**) Neurologic evaluation was assessed daily after reperfusion until the rats were killed. (**B**, **C**) Spontaneous motor activity was evaluated by the rota-rod test before MCAO (pre) and at 2 and 5 days after MCAO. (**B**) Comparison of endurance on the rotating rod. (**C**) Time-dependent changes in the percentage (%) of walking rats on the rotating rod before MCAO (preperformance) and at 2 and 5 days after MCAO. (**D**, **E**) The number of full-turn rotations in the ipsilateral direction was counted every 5 mins (**D**) for 60 mins (**E**) after the intraperitoneal administration of methamphetamine (2.5 mg/kg) at 6 days after MCAO. Data are the mean ± s.e.m. Significance (Scheffe's *post hoc* comparisons after Kruskal–Wallis test or Bonferroni/Dunn *post hoc* comparisons after ANOVA): $^{*}P < 0.05$, $^{**}P < 0.01$ versus PBS-injected ischemic rats. $^{\dagger}P < 0.05$, $^{\dagger\dagger}P < 0.01$ versus GST-injected ischemic rats.

injection, and then the rats showed stable rotation of approximately 30 turns for 5 mins (Figure 3D). The total number of rotations in 60 mins reached 300 turns in PBS- and GST-injected rats. In contrast, the total number of rotations in GST-DJ-1-injected rats was significantly reduced (Figure 3E).

Changes in Immunoreactivities for Microtubule-Associated Protein-2, Tyrosine Hydroxylase, and Nitrotyrosine

It is known that damaged tissues sometimes cause nonspecific staining. To reduce this possibility, we

usually performed the incubation at 4°C (in a cold room) with a lower concentration of primary antibody. In addition, when brain slices were incubated with mouse IgG1 or rabbit IgG as control, instead of the primary antibody, nonspecific staining was undetectable in the ischemic core and in the boundary zone of the ischemic region, under our experimental condition (Supplementary Figure S3).

At 7 days after MCAO, the treated rats were killed. For immunohistochemical analysis, sections were prepared and immunostaining with antibodies against MAP2, TH, and nitrotyrosine was performed. In sham-operated rats, although MAP2 immunoreactivity was detected in the cerebral cortex and the striatum (Figures 4A and 4E), this immunoreactivity was markedly reduced in the ipsilateral cerebral cortex and the striatum in PBS- and GST-injected rats (Figures 4B, 4C, 4F, and 4G). In contrast, GST-DJ-1-injected rats showed a reduction in the loss of MAP2 immunoreactivity in both the cerebral cortex and the striatum (Figures 4D and 4H). In addition, we evaluated TH immunoreactivity as an index of the level of dopaminergic neuronal injury. Presynaptic and neural fiber TH immunoreactivity was mainly detected in the striatum (Figure 4I), and TH-immunopositive neural cell bodies were detected in the SNpc in sham-operated rats (Figure 4M). Although fibrillar TH immunoreactivity in the striatum and the number of TH-immunopositive neurons in the SNpc were reduced by MCAO (Figures 4J, 4K, 4N, and 4O), these reductions were markedly inhibited in GST-DJ-1-injected rats (Figures 4L and 4P). By semiquantitative analysis, similar results were obtained (Supplementary Figure S4).

However, normal rats that were injected with GST-DJ-1 did not exhibit any abnormal behavior (data not shown). In addition, as MAP2-immunoreactive neural fibers in GST-DJ-1-injected ipsilateral hemisphere did not change for 7 days after injection (Supplementary Figure S5), GST-DJ-1 may not affect naive neurons.

We further estimated nitrotyrosine immunoreactivity as an index of the level of oxidative and nitrosative stress. Although immunoreactivity for nitrotyrosine was hardly detected in sham-operated rats (Figures 5A, 5E, 5I, and 5M), this immunoreactivity was markedly increased in PBS- and GST-injected rats in the boundary zones of the ischemic core in the cerebral cortex and the striatum and in the ischemic core in the striatum (Figures 5B, 5C, 5F, 5G, 5J, 5K, 5N, and 5O). In contrast, in GST-DJ-1-injected rats, the number of nitrotyrosine-immunopositive cells was significantly reduced in the boundary zones of the ischemic core in the cerebral cortex and striatum, but not in the ischemic core in the striatum (Figures 5D, 5H, 5L, 5P, 5Q, 5R, and 5S).

Distribution of Glutathione *S*-Transferase-Tagged Human DJ-1 after Intrastriatal Injection

To investigate the distribution of exogenous human DJ-1 in the rat brain, we performed the intrastriatal injection of GST-DJ-1 (320 pmol). Exogenous GST-DJ-1 was then detected using an anti-GST antibody.

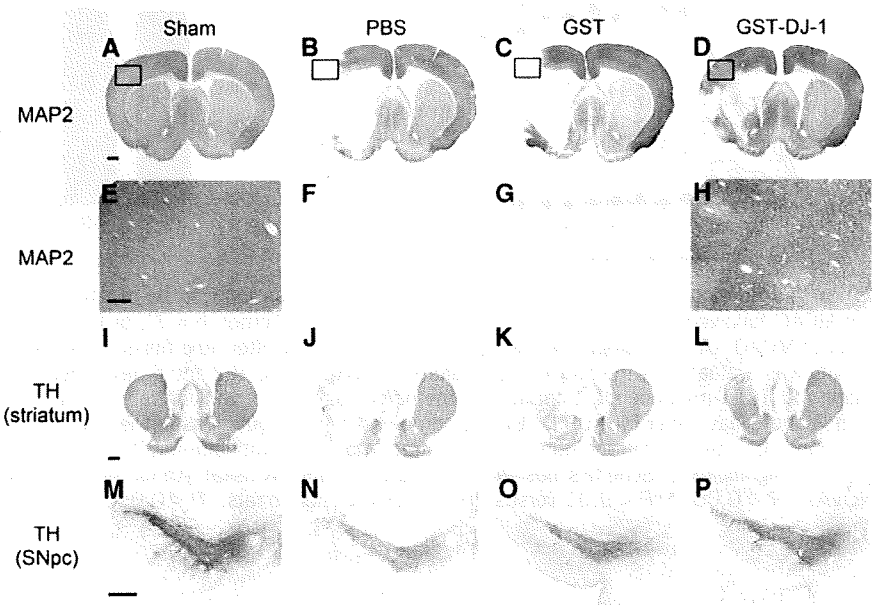

Figure 4 Immunohistochemical changes after the injection with GST-tagged human DJ-1 (GST-DJ-1) in ischemic rats. (**A** to **P**) Representative photographs showing brain sections at + 1 (**A** to **L**) and −5 (**M** to **P**) mm anterior–posterior from the bregma, which were immunostained with antibodies against MAP2 (**A** to **H**) and TH (**I** to **P**) in sham-operated rats (**A**, **E**, **I**, and **M**) and ischemic rats at 7 days after MCAO, which had been injected with PBS (**B**, **F**, **J**, and **N**), GST (320 pmol) (**C**, **G**, **K**, and **O**), or GST-DJ-1 (320 pmol) (**D**, **H**, **L**, and **P**) at 110 mins after the onset of MCAO. (**E** to **H**) High-magnification images are indicated in (**A** to **D**). Scale bars: 1 mm (**A** to **D** and **I** to **L**), 200 μm (**E** to **H**), and 500 μm (**M** to **P**).